Simulation of a spin-stabilised sports disc

W.J. Crowther and J.R. Potts

School of Mechanical, Aerospace & Civil Engineering, University of Manchester, Manchester, UK

Abstract

The spin-stabilised sports disc, more commonly known as the Frisbee, is used for a variety of recreation and sporting activities. Frisbees have unique flying characteristics compared to other sports projectiles because they depend on spin for stability during flight and, at typical launch speeds, aerodynamic lift is greater than or equal to the weight of the disc. In this paper, a six degree of freedom mathematical model of a spinning disc wing is developed and a simple analytical expression derived for the disc roll rate in straight and level flight. It is shown that dimensionless disc trajectories will be similar for similar values of a parameter based on the ratio of the disc static margin to the disc advance ratio. The mathematical model is implemented as a simulation in Matlab using steady model parameters obtained from wind tunnel tests and unsteady parameters from flight tests. Simulation results are shown to be in reasonable agreement with limited available experimental flight data. The effect of launch conditions has been investigated using a series of numerical experiments. It is found that flight path curvature in the horizontal plane increases with decreasing advance ratio, as expected. Pitch angles at launch for maximum range and maximum duration are approximately 10° and 20° respectively. Also, the locus of disc landing position as a function of launch roll angle has been shown to be an 'S' shaped curve, with the straightest flight occurring for an initial roll angle of –6°. Finally, the simulation has been extended to include the effects of hypothetical control inputs, enabling simulation of novel Frisbee manoeuvres.

Keywords: aerodynamics, Frisbee, modelling, simulation, sports disc, trajectory

Nomenclature

$AdvR$	advance ratio
c	disc diameter (m)
C_{Drag}	drag coefficient
$\mathbf{C}_F$	aerodynamic force coefficient vector
C_L	rolling moment coefficient
C_{Lift}	lift coefficient
C_{Lp}	roll damping coefficient
C_M	pitching moment coefficient
$\mathbf{C_M}$	aerodynamic moment coefficient vector
$C_{M_{cg}}$	pitching moment coefficient about centre of gravity
C_N	yawing moment coefficient
C_{M_q}	pitch damping coefficient
C_{N_r}	yaw damping coefficient
C_{Side}	side force coefficient
$\mathbf{F}$	force vector (N)
g	acceleration due to gravity (m s^{-2})
I_x, I_y, I_z	moments of inertia (kg m^2)

Correspondence address:
W.J. Crowther
School of Mechanical, Aerospace & Civil Engineering
University of Manchester
Manchester M60 1QD
UK
Tel: +44 161 2754333
E-mail: w.j.crowther@man.ac.uk

I	moment of inertia matrix (kg m^2)
$\mathbf{k}_n$	static margin
ℓ	length scale (m)
L, M, N	rolling, pitching and yawing moments (N m)
m	mass of disc wing (kg)
$\mathbf{M}$	moment vector (N m)
p, q, r	body axis roll, pitch and yaw rates (rad s^{-1})
q_∞	dynamic pressure (N m^{-2})
S	planform area (m^2)
t	time (s)
$\mathbf{T}_a$	transformation matrix (forces and velocities)
$\mathbf{T}_r$	transformation matrix (angular rates)
u, v, w	body axis velocity components (m s^{-1})
V_∞	freestream wind speed (m s^{-1})
x, y, z	generic coordinate system
X, Y, Z	displacements in Earth axes (m)
$\mathbf{x}$	position vector (m)
α	angle of attack (rad)
β	angle of sideslip (rad)
λ	absolute attitude angle (rad)
ϕ, θ, ψ	roll, pitch and yaw Euler angles (rad)
$\mathbf{\Theta}$	Euler orientation vector
ρ_∞	air density (kg m^{-3})
$\tilde{\omega}$	angular velocity matrix (rad s^{-1})
Ω	spin rate about disc normal (rad s^{-1})

Subscripts

$_1$	earth axes
$_2$	body axes
$_3$	zero sideslip body axes
$_4$	zero sideslip wind axes
$_{aero}$	aerodynamic component
$_{control}$	aerodynamic control input
$_L$	launch

Superscripts

^{T}	transpose

Embellishments

$\hat{}$	dimensionless variable or unit vector

Abbreviations

AoA	angle of attack
cg	centre of gravity
cp	centre of pressure

Introduction

The spin-stabilised sports disc, most generally known as the Frisbee, is used for a wide range of sporting activities, from casual recreational flying to Disc Golf , and the team game of Ultimate. Its flight characteristics are unique compared to other sports projectiles for a number of reasons. Firstly, under typical flight conditions, it is possible to generate a lift force greater than or equal to the weight of disc. Secondly, this lift force is appreciably greater than the drag force and, finally, the disc dynamics are dominated by gyroscopic effects due to spin. It is these characteristics that enable the Frisbee to demonstrate the stable, horizontal, gliding flight that is the key to its widespread use in sport and recreation.

The Frisbee is part of a wider class of projectiles known as spin-stabilised disc wings, which also includes the discus (Bartlett, 1992) and clay pigeon (Peterson, 1971). Typically, spin-stabilised disc-wing projectiles are rotationally symmetric, which implies that the centre of gravity is at the disc centre. The clay pigeon has similar geometry to that of a Frisbee, however tends to be smaller and has a higher wing loading (ratio of weight to planform area), enabling efficient flight at the higher velocities required for game bird simulation. The discus, on the other hand, has upper–lower surface symmetry and increased wing loading to the point where aerodynamic lift is small compared to gravitational forces at typical flight speeds.

The goal of the present paper is to develop a framework for simulating the dynamics of spin-stabilised flying sports discs. The approach is generic in that it is applicable to any spin-stabilised disc wing for which the mass and aerodynamic properties are known. This paper will focus on the results for a typical sports disc for which a comprehensive database of steady aerodynamic data was available for the complete angle of attack range (0–90°) (Potts, 2005). Unsteady aerodynamic derivatives (damping due to pitch, roll and yaw rate) are estimated from values in the literature (Hummel, 2003).

Previous work relevant to the present paper is divided into a number of interrelated areas. Firstly, there is the measurement of aerodynamic properties of disc wings directly using wind tunnel experiments (Yasuda, 1999; Mitchell, 1999) and indirectly from free-flight experiments (Hubbard & Hummel, 2000).

Secondly, there is the development of numerical simulation models of disc-wing flight (Hubbard & Hummel, 2000), which is related to the first area in that a (linearised) dynamic model of some sort is required for identification of parameters from flight tests. Finally, there is the literature associated with the biomechanics of discus- or Frisbee-throwing (Bartlett, 1992; Hubbard & Hummel, 2001). The latter provides useful information on the range of launch conditions (attitude, velocity and spin rate) physically possible and, coupled with the use of simulation, allows their optimisation for specific performance goals.

Until recently, the published wind tunnel data on Frisbee aerodynamics was relatively limited (Stilley & Carstens, 1972), especially with respect to the pitching moment characteristic with angle of attack, which is critical to the flight behaviour of a spin-stabilised disc wing. In response to this, a comprehensive wind tunnel test programme was undertaken at the University of Manchester as part of a PhD study (Potts, 2005). It is this data that is used for the present simulation work.

Estimation of parameters from flight tests (Hummel, 2003) is significantly more challenging than wind tunnel testing and there is considerable scatter in the results obtained. Furthermore, it is only possible to obtain parameters linearised around a nominal flight condition. That said, the only experimental data currently available on the rate damping derivatives (Hummel & Hubbard, 2002, 2004) is from flight tests, meaning the technique provides an important input for simulation work.

Recent work by Lorenz (2005) has reported free flight experiments on a Frisbee instrumented for acceleration, attitude (optical and magnetic) and qualitative measurements of pressure. This is a promising line of work that will deliver increasingly useful results as the technique matures.

A number of disc-wing simulation studies have been previously published. The earliest of these was by Katz (1968) who simulated the free flight of a rotating disc. There have also been a number of early studies investigating the effect of launch conditions on discus trajectories (Frohlich, 1981; Soong, 1976). More recently, Hubbard & Hummel (2000) developed a 5dof Frisbee simulation and demonstrated basic Frisbee flight trajectories successfully. Hummel (2003) compared simulated trajectories to experimental flight path data, as did the authors (Potts, 2005), to validate the simulation. The present paper moves beyond model validation to present simulated experiments to show the effect of varying advance ratio, angle of attack, pitch angle and roll angle at launch. The effect of fixed control inputs to simulate turn manoeuvres is also given.

Theory

Disc-wing equations of motion

The disc-wing simulation is based on the standard equations of motion of a rigid flight vehicle in three dimensions (Etkin & Reid, 1996). The standard equations of motion are cast using two axes systems: Earth-fixed (earth axes) and body-fixed (body axes). The two systems are related by a displacement vector $\mathbf{x}_1$ and a sequence of rotations defined by the Euler angles ϕ, θ and ψ. For the present work the Euler angle sequence is applied in the conventional order of yaw, pitch, roll, Fig. 1. Due to the rotational symmetry of a disc wing, some mathematical simplification may be made by adopting a non-standard Euler angle sequence in which the yaw rotation is applied last.

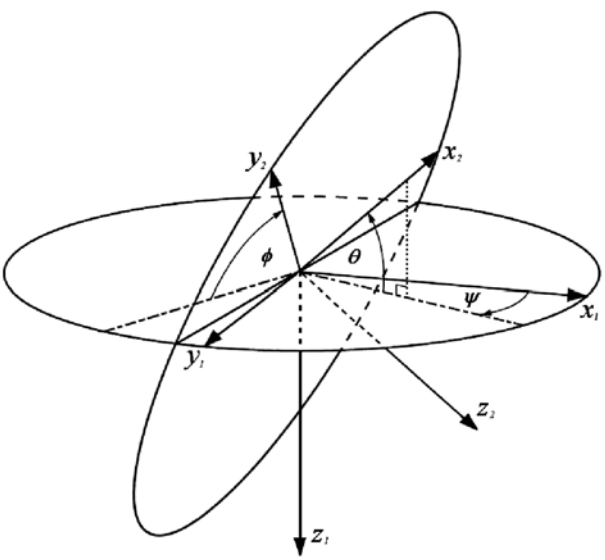

Figure 1 Relationship between earth axes $(xyz)_1$ and body axes $(xyz)_2$ coordinate systems defined in terms of the Euler angles ϕ, θ, ψ. Note that the rotations are applied in the order ψ, θ, ϕ about the *x*, *y* and *z* axes respectively.

While this approach has its merits, it was not adopted in order to maintain compatibility with previous work both by the authors and in the literature that uses the standard Euler sequence.

For simulation of aircraft, it is usually convenient to define the orientation of the wind vector with respect to the body axes using two aerodynamic angles, namely angle of attack and angle of sideslip. An aerodynamic model is then built up from a data matrix covering the range of angles of attack and sideslip of interest. Due to the nature of the rotational symmetry of a disc wing, the angle of sideslip is redundant, and a complete aerodynamic model can be defined solely using the angle of attack in what is referred to as the absolute incidence plane. In order to implement this aerodynamic model conveniently as part of the standard equations of motion, it useful to define an additional two axes systems for the disc wing, namely the zero sideslip body axes and the zero sideslip wind axes. The four axes systems used are notated as follows:

1 Earth axes $(xyz)_1$
2 Body axes $(xyz)_2$
3 Zero sideslip body axes $(xyz)_3$
4 Zero sideslip wind axes $(xyz)_4$

The relationship between the last three of these axes systems is illustrated in Fig. 2. Note that the zero sideslip body axes are obtained by rotating the body axes through the sideslip angle. The zero sideslip wind axes are then obtained by rotating the zero sideslip body axes through the angle of attack.

In order to transform vector components between different axes systems, a series of transformations are defined. To simplify presentation, a subscript notation system is adopted where for a given transformation matrix $\mathbf{T}$, the first subscript defines whether the transform is an attitude transform (subscript a) or an angular rate transform (subscript r) and the subsequent numerical subscripts define the axes between which the transformation takes place. For example, the attitude transformation between earth axes (system 1) and body axes (system 2) is written as $\mathbf{T}_{a_{12}}$.

A general expression for $\mathbf{T}_a$ is obtained by combining a sequence of rotations ϕ, θ and ψ about the x, y and z axes respectively of the initial axes system:

$$\mathbf{T}_a(\phi, \theta, \psi) = \left[\begin{bmatrix} 1 & 0 & 0 \\ 0 & \cos\phi & -\sin\phi \\ 0 & \sin\phi & \cos\phi \end{bmatrix}\begin{bmatrix} \cos\theta & 0 & \sin\theta \\ 0 & 1 & 0 \\ -\sin\theta & 0 & \cos\theta \end{bmatrix}\begin{bmatrix} \cos\psi & -\sin\psi & 0 \\ \sin\psi & \cos\psi & 0 \\ 0 & 0 & 1 \end{bmatrix}\right]^T \quad (1)$$

Note that the transformation definition used means that this matrix is equivalent to the standard form of the directional cosine matrix widely used to define orientation across a range of disciplines, including computer graphics and rigid body dynamics.

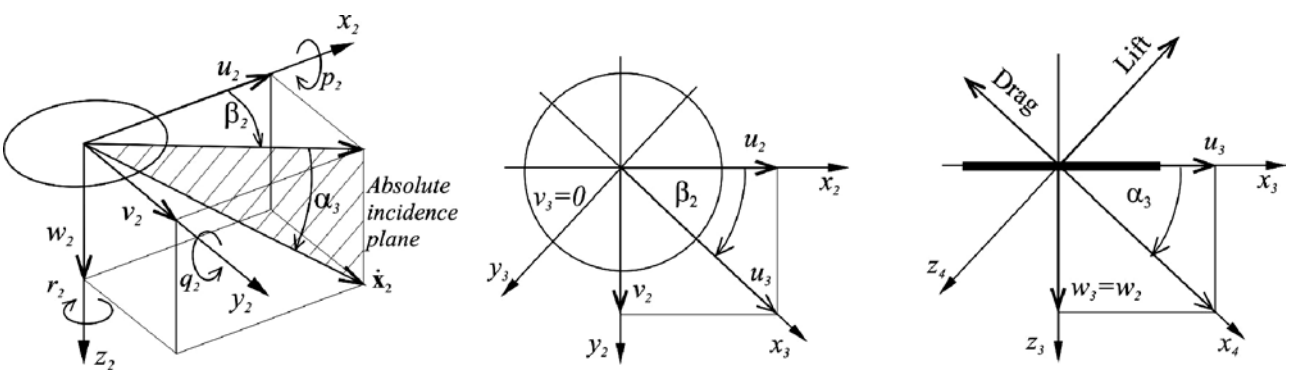

(a) Body axes $(xyz)_2$, isometric view

(b) Zero sideslip body axes $(xyz)_3$, view looking along z_3

(c) Zero sideslip wind axes $(xyz)_4$, view looking along $-y_4$

Figure 2 Graphical definition of disc-wing axes systems.

The specific transformations used for the present work are then defined as:

$$\mathbf{T}_{a_{12}}(\phi, \theta, \psi) = \begin{bmatrix} \cos\phi\cos\psi & \sin\phi\sin\theta\cos\psi + \cos\phi\sin\psi & -\cos\phi\sin\theta\cos\psi + \sin\phi\sin\psi \\ \cos\theta\sin\psi & \sin\phi\sin\theta\sin\psi + \cos\phi\cos\psi & \cos\phi\sin\theta\sin\psi + \sin\phi\cos\psi \\ \sin\theta & -\sin\phi\cos\theta & \cos\phi\cos\theta \end{bmatrix}, \quad (2)$$

$$\mathbf{T}_{a_{23}}(0, 0, \beta) = \begin{bmatrix} \cos\beta & -\sin\beta & 0 \\ -\sin\beta & \cos\beta & 0 \\ 0 & 0 & 1 \end{bmatrix} \quad (3)$$

and

$$\mathbf{T}_{a_{34}}(0, \alpha, 0) = \begin{bmatrix} \cos\alpha & 0 & -\sin\alpha \\ 0 & 1 & 0 \\ \sin\alpha & 0 & \cos\alpha \end{bmatrix}. \quad (4)$$

Note that by definition,

$$\mathbf{T}_{a_{21}}(\phi, \theta, \psi) = \mathbf{T}_{a_{12}}(-\phi, -\theta, -\psi) = \mathbf{T}_{a_{12}}(\phi, \theta, \psi)^T \quad (5)$$

Body axes rates are transformed to Euler rates via the following matrix,

$$\mathbf{T}_{r_{21}}(\phi, \theta, \psi) = \begin{bmatrix} 1 & 0 & -\sin\theta \\ 0 & \cos\phi & \cos\theta\sin\psi \\ 0 & -\sin\phi & \cos\theta\cos\psi \end{bmatrix}. \quad (6)$$

The position and orientation of the disc-wing is defined by a position vector $\mathbf{x}$ and attitude vector $\boldsymbol{\theta}$. Using standard aircraft notation,

$$\mathbf{x}_1 = [X\ Y\ Z]^T, \qquad \boldsymbol{\theta}_1 = [\phi\ \theta\ \psi]^T \quad (7)$$

and

$$\dot{\mathbf{x}}_2 = [u\ v\ w]^T, \qquad \dot{\boldsymbol{\theta}}_2 = [p\ q\ r]^T. \quad (8)$$

Furthermore, using the transformations defined above,

$$\dot{\mathbf{x}}_2 = \mathbf{T}_{a_{21}}\dot{\mathbf{x}}_1, \qquad \dot{\boldsymbol{\theta}}_2 = \mathbf{T}_{r_{12}}, \dot{\boldsymbol{\theta}}_1. \quad (9)$$

The system dynamics are governed by Newton's Second Law which, using the notation defined by Etkin & Reid (1982), can be conveniently expressed as,

$$\ddot{\mathbf{x}}_2 = \frac{\mathbf{F}_2}{m} - \tilde{\omega}\dot{\mathbf{x}}_2, \quad (10)$$

and

$$\ddot{\theta}_2 = \mathbf{I}^{-1}\left(\mathbf{M}_2 - \tilde{\omega}\mathbf{I}\dot{\boldsymbol{\theta}}_2\right), \quad (11)$$

where $\mathbf{F}_2$ and $\mathbf{M}_2$ are the body axes force and moment vectors acting on the disc, m is the disc mass, $\mathbf{I}$ is the disc moment of inertia matrix defined as,

$$\mathbf{I} = \begin{bmatrix} I_x & 0 & 0 \\ 0 & I_y & 0 \\ 0 & 0 & I_z \end{bmatrix}, \quad I_x = I_y. \quad (12)$$

and

$$\tilde{\boldsymbol{\omega}} = \begin{bmatrix} 0 & -r & q \\ r & 0 & -p \\ -q & p & 0 \end{bmatrix} \quad (13)$$

such that,

$$\dot{\boldsymbol{\theta}}_2 \times \dot{\mathbf{x}}_2 = \tilde{\boldsymbol{\omega}}\dot{\mathbf{x}}_2, \qquad \dot{\boldsymbol{\theta}}_2 \times \mathbf{I}\dot{\boldsymbol{\theta}}_2 = \tilde{\boldsymbol{\omega}}\mathbf{I}\dot{\boldsymbol{\theta}}_2. \quad (14)$$

Eqn. 11 is an exact expression of conservation of angular momentum, and as such it is implicit that the body fixed axes $(xyz)_2$ rotate with the disc. In order to investigate means of reducing the computational time for the model, the physics of the problem was simplified by assuming that the time rate of change of the spin rate was zero ($\dot{r} = 0$), meaning that the disc spin rate was a constant equal to the initial spin rate of the disc, denoted Ω. The imposition of constant spin rate reduces the order of the dynamic model obtained in that angular momentum can now no longer be exchanged between the spin axis and pitch/roll axes. This eliminates the relatively high frequency disc 'wobble' mode that is stable but under damped and in so doing greatly reduces the computational effort

required to numerically integrate the model. The wobble mode is typically excited by poorly coordinated launch conditions in which the initial spin vector is not exactly normal to the disc; for a correctly coordinated disc launch there is no wobble. For the purposes of discussion, the disc-wing model based on the exact angular momentum equation will be referred to as the exact model, whereas the model based on an assumption of constant spin rate will be referred to as the constant spin rate model. The scalar equation form of these two models is presented later in this section, and comparison of the difference in numerical results from each of the models discussed discussed under 'Simulation implementation'. Note that the results presented in this paper are based on using the constant spin rate model unless otherwise stated.

The principal task in solving the disc-wing equations of motion (eqns. 10 and 11) is now that of obtaining the aerodynamic forces and moments acting on the disc-wing as a function of its velocity, aerodynamic attitude and rate. The approach adopted is as follows.

With reference to Fig. 2, calculate the sideslip angle of the disc within the body axes system using the four-quadrant inverse tangent,

$$\beta_2 = \text{atan } 2\left(\frac{\dot{\mathbf{x}}_2(2)}{\dot{\mathbf{x}}_2(1)}\right). \tag{15}$$

Next, use this result to determine the transform between body axes and zero sideslip body axes (eqn. 3), and hence calculate the velocity in the zero sideslip body axes system,

$$\dot{\mathbf{x}}_3 = \mathbf{T}_{a_{23}}\dot{\mathbf{x}}_2. \tag{16}$$

From this, calculate the disc absolute incidence, as follows,

$$\alpha_3 = \text{atan } 2\left(\frac{\dot{\mathbf{x}}_3(3)}{\dot{\mathbf{x}}_3(1)}\right), \tag{17}$$

with the orientation of the zero sideslip wind axes given by

$$\dot{\mathbf{x}}_4 = \mathbf{T}_{a_{34}}\dot{\mathbf{x}}_3. \tag{18}$$

The aerodynamic force and moment coefficients can now be obtained either from linear aerodynamic derivatives (Hubbard & Hummel, 2000) or, as in the present case, a mixture of linear derivatives for the rate terms and look up table results based on wind tunnel experiments for the steady terms. The complete set of force and moment coefficients used is as follows,

$$C_{Drag} = C_{Drag}(\alpha_3), \tag{19}$$

$$C_{Lift} = C_{Lift}(\alpha_3), \tag{20}$$

$$C_{Side} = C_{Side}(r_3, V_\infty), \tag{21}$$

$$C_L = C_{L_p}\frac{p_3 c}{2V_\infty} \tag{22}$$

$$C_M = C_M(\alpha_3) + C_{M_q}\frac{q_3 c}{2V_\infty} \tag{23}$$

$$C_N = C_{N_r}\frac{r_3 c}{2V_\infty} \tag{24}$$

where,

$$\dot{\boldsymbol{\theta}}_3 = [p_3\ q_3\ r_3]^T \tag{25}$$

A sample set of longitudinal wind tunnel data is shown in Fig. 3, from Potts & Crowther (2002). These graphs also show a linear fit to the data, based on a set of linearised aerodynamic derivatives obtained at a 5° angle of attack. Notice that linear fit is quite good for lift and drag, but relatively poor for pitching moment for angles of attack greater than 10° and less than 0°. The difference between simulation results obtained with the steady linear derivatives and results obtained using the full non-linear steady data is discussed discussed under the heading 'Analysis of a typical Frisbee trajectory'. Values used for the unsteady pitch and roll damping derivatives $C_{M_q} = -1.40$, $C_{L_p} = -1.30$ were obtained from Hummel (2003).

Once the coefficients are known, the dimensional forces and moments acting on the disc are then given by

$$\mathbf{F}_4 = q_\infty S\mathbf{C}_\mathrm{F} \tag{26}$$

and

$$\mathbf{M}_4 = q_\infty Sc\mathbf{C}_\mathrm{M} \tag{27}$$

where

$$\mathbf{C}_\mathrm{F} = \left[-C_{Drag}\ C_{Side}\ -C_{Lift}\right], \tag{28}$$

$$\mathbf{C}_\mathrm{M} = \left[C_L\ C_M\ C_N\right] \tag{29}$$

and

$$q_\infty = \frac{1}{2}\rho_\infty V_\infty^2, \qquad V_\infty = \left|\dot{\mathbf{x}}_1\right|. \tag{30}$$

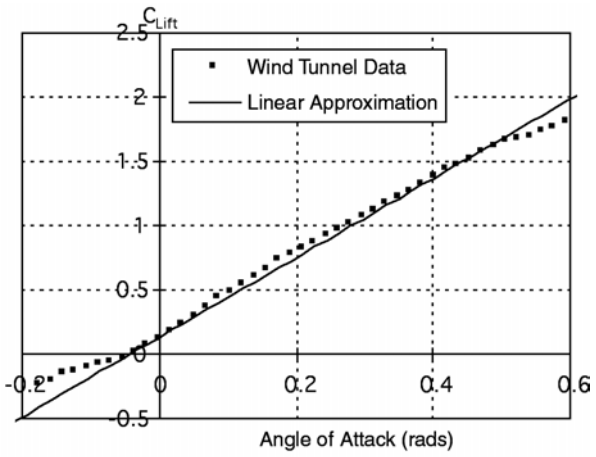

(a) Lift coefficient.

$$C_{Lift} = C_{Lift_0} + C_{Lift_\alpha}\alpha \qquad \left[C_{Lift_0} = 0.13,\ C_{Lift_\alpha} = 3.09\right]$$

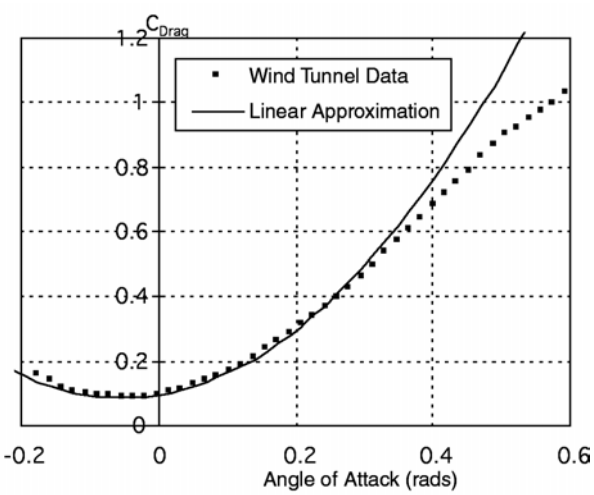

(b) Drag coefficient.

$$\left[C_{Drag_0} = 0.085,\ C_{Drag_\alpha} = 3.30,\ \alpha_0 = -0.052\right]$$

$$C_{Drag} = C_{Drag_0} + C_{Drag_\alpha}(\alpha - \alpha_0)^2$$

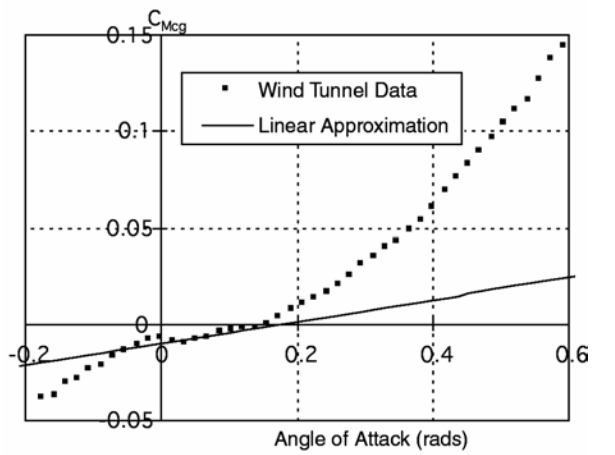

(c) Pitching moment coefficient.

$$C_M = C_{M_0} + C_{M_\alpha}\alpha \qquad \left[C_{M_0} = -0.01,\ C_{M_\alpha} = 0.057\right]$$

Figure 3 Wind tunnel data (symbols) for a Frisbee-like disc wing, used to model aerodynamic forces and moments in the simulation. Lines indicate data linearised around typical flight angle of attack.

The forces and moments now have to be resolved back in to body axes. This is achieved as follows:

$$\mathbf{F}_{2(aero)} = \mathbf{T}_{a_{23}}{}^T \mathbf{T}_{a_{34}}{}^T \mathbf{F}_4 \tag{31}$$

$$\mathbf{M}_2 = \mathbf{T}_{a_{23}}{}^T \mathbf{T}_{a_{34}}{}^T \mathbf{M}_4. \tag{32}$$

Finally, gravitational forces have to be added:

$$\mathbf{F}_2 = \mathbf{F}_{2(aero)} + \mathbf{T}_{a_{12}}{}^T m\mathbf{g} \tag{33}$$

where,

$$\mathbf{g} = [0\ 0\ g]^T. \tag{34}$$

Note that gravitational moments are zero since the moment reference point is the centre of gravity.

Eqns. 10 and 11 can now be integrated, via suitable axes transformation, to give the earth axes position and orientation as required.

The complete equations of motion are given in scalar form in eqns. 35–40 below. Note that these equations are written with respect to the disc body axes $(xyz)_2$ and include reference to the sideslip angle (β_2) and the absolute incidence (α_3). For the purposes of linear analysis, these equations can be simplified by

considering the case where $\beta_2 = \alpha_3 = 0$. This leads to eqns. 41–46, which are consistent with those derived by Lissaman (1998). Finally, the scalar form of the constant spin rate version of the moment equations can be obtained by setting $r = \Omega$ and $\dot{r} = 0$ in eqns. 44–46, giving eqns. 47–49.

$$q_\infty S\left(-C_{Drag}\cos\beta_2\cos\alpha_3 - C_{Side}\sin\beta_2 - C_{Lift}\cos\beta_2\sin\alpha_3\right) + mg\sin\theta = m\left(\dot{u} + qw - rv\right) \quad (35)$$

$$q_\infty S\left(-C_{Drag}\sin\beta_2\cos\alpha_3 - C_{Side}\cos\beta_2 - C_{Lift}\sin\beta_2\sin\alpha_3\right) - mg\cos\theta\sin\phi = m\left(\dot{v} + ru - pw\right) \quad (36)$$

$$q_\infty S\left(C_{Drag}\sin\alpha_3 - C_{Lift}\cos\alpha_3\right) + mg\cos\theta\cos\phi = m\left(\dot{w} + pv - qu\right) \quad (37)$$

$$q_\infty Sc\left(C_L\cos\beta_2\cos\alpha_3 - C_M\sin\beta_2 + C_N\cos\beta_2\sin\alpha_3\right) = I_x\dot{p} + qr\left(I_z - I_y\right) \quad (38)$$

$$q_\infty Sc\left(C_L\sin\beta_2\cos\alpha_3 + C_M\cos\beta_2 + C_N\sin\beta_2\sin\alpha_3\right) = I_y\dot{q} + rp\left(I_x - I_z\right) \quad (39)$$

$$q_\infty Sc\left(-C_L\sin\alpha_3 + C_N\cos\alpha_3\right) = I_z\dot{r} \quad (40)$$

$$-q_\infty SC_{Drag} + mg\sin\theta = m\dot{u} \quad (41)$$

$$q_\infty SC_{Side} - mg\cos\theta\sin\phi = m\left(\dot{v} + ru\right) \quad (42)$$

$$-q_\infty SC_{Lift} + mg\cos\theta\cos\phi = m\left(\dot{w} - qu\right) \quad (43)$$

$$q_\infty ScC_L = I_x\dot{p} + qr(I_z - I_y) \quad (44)$$

$$q_\infty ScC_M = I_y\dot{q} + rp(I_x - I_z) \quad (45)$$

$$q_\infty ScC_N = I_z\dot{r} \quad (46)$$

$$q_\infty ScC_L = I_x\dot{p} + q\Omega(I_z - I_y) \quad (47)$$

$$q_\infty ScC_M = I_y\dot{q} + \Omega p(I_x - I_z) \quad (48)$$

$$\dot{r} = 0 \quad (49)$$

The gravitational terms in the above equations of motion depend both on the pitch and roll angle of the disc. However, due to disc rotational symmetry, there exists a coordinate system in which the gravitational forces depend on a single angle, namely the absolute attitude, λ, defined as the angle between the unit gravity vector and the disc normal:

$$\cos\lambda = \hat{\underline{z}}_1.\hat{\underline{z}}_2 = \cos\phi\cos\theta. \quad (50)$$

The absolute attitude is also consistent with the way humans perceive disc attitude, and will be used in preference to the Euler angles to describe attitude when presenting trajectory results in the Results section.

Simplified flight dynamics of a spin-stabilised disc

The most distinctive feature of disc-wing flight compared to the flight of other projectiles or aircraft is the tendency for disc-wings to roll about their direction of motion due to gyroscopic effects. This tendency is known anecdotally as the 'turnover effect' (Schuurmans, 1990). In the following, a simplified analysis of disc-wing flight is used to derive expressions for the disc roll and pitch rate as a function of applied pitching and rolling moments. The starting point for the analysis is the equations of motion as defined by eqns. 41–46. Assuming a horizontal flight path, equilibrium of forces and negligible yawing moment (a reasonable assumption based on flight test experimental results), the equations reduce down to the rolling moment and pitching moment equations:

$$L = I_x\dot{p} + qr(I_z - I_y), \quad (51)$$

$$M = I_y\dot{q} + rp(I_x - I_z). \quad (52)$$

If it is assumed, furthermore, that the angular motion of the disc is unaccelerated (once again a reasonable assumption from flight test experiments) such that $\dot{p} = \dot{q} = \dot{r} = 0$, and that the disc is thin, uniform and axisymmetric such that $I_x = I_y = \frac{1}{2}I_z$, then eqns. 51–52 reduce to:

$$q = \frac{2L}{rI_z} \quad (53)$$

$$p = \frac{2M}{rI_z}. \quad (54)$$

These equations express the fundamental effect of gyroscopic precession on the dynamics of a disc-wing, i.e. for a positive spin rate, a positive rolling moment causes pitch up and a positive pitching moment causes roll left wing down. Since the aerodynamic rolling moment on a symmetrical disc is very small (Potts, 2005), the precessional pitch rate is negligible. However, the pitching moment acting on a disc-wing may be quite large and hence the roll rate can be significant.

Non-dimensional analysis

It is proposed that dimensionless disc-wing trajectories from similar starting conditions will be nominally similar if the dimensionless roll rate is similar. The following analysis briefly outlines the derivation of a dimensionless roll rate parameter. The similarity of flight trajectories is discussed under the heading 'Flight path similarity for similar dimensionless roll rates'. It is anticipated that this work can be used as the starting point for more comprehensive disc-wing dynamic stability studies in the future.

In keeping with standard practice for flight vehicle analysis, define dimensionless time $\hat{t}$ and dimensionless distance $\hat{\ell}$ as follows:

$$\hat{t} = \frac{tg}{V_\infty} \tag{55}$$

$$\hat{\ell} = \frac{\ell g}{V_\infty^2}. \tag{56}$$

From eqn. 54, the dimensionless disc roll rate is obtained as follows,

$$\hat{p} = \frac{pV_\infty}{g} = \frac{2MV_\infty}{rI_z g}. \tag{57}$$

Assuming that M_0 for the disc is zero (which is not true in practice), the disc pitching moment can be approximated by

$$M = -k_n C_{Lift} q_\infty Sc, \tag{58}$$

where k_n is the static margin, defined as

$$k_n = -\frac{\partial C_{M_{cg}}}{\partial C_{Lift}}. \tag{59}$$

The disc's mass moment of inertia about the z-axis will depend on the mass distribution of the disc, with typically most of the mass concentrated round the outer edge. For the present analysis, however, it is assumed that the disc is a uniform circular cylinder of negligible height for which,

$$I_z = \frac{1}{8} mc^2, \tag{60}$$

where m is the overall mass of the disc.

Substituting eqns. 58 and 60 into eqn. 57, the following result is obtained:

$$\hat{p} = \frac{16 k_n C_{Lift} q_\infty SV_\infty}{mg\, rc}. \tag{61}$$

Given that for the condition Lift = Weight,

$$C_{Lift} = \frac{mg}{q_\infty S} \tag{62}$$

and that,

$$AdvR = \frac{rc}{2V_\infty} \tag{63}$$

eqn. 61 further simplifies to,

$$\hat{p} = \frac{8k_n}{AdvR}. \tag{64}$$

Eqn. 64 states that, within the limitation of the stated assumptions, the dimensionless roll rate of a disc-wing in unaccelerated horizontal flight is proportional to the ratio of static margin to the advance ratio. Thus roll rate is minimised when:

1 The static margin, k_n, of the disc is minimised, and
2 The disc is launched with a high spin rate compared to the forward velocity (high advance ratio).

The static margin of a disc-wing at typical flight angles of attack is primarily a function of cross-sectional profile. Experimental studies (Potts, 2005) have shown that for high quality discs, the aerodynamic centre is usually close to the centre of the disc, and hence the static margin is small, minimising the disc turn over effect. Poorer quality discs often have a significant static margin and hence roll more rapidly in flight. A good thrower, however, can compensate for this by spinning the disc at a greater rate for the same launch speed.

Simulation implementation

A number of numerical experiments based on typical launch conditions were performed to evaluate the difference between the exact disc-wing model and the constant spin rate model. It was found that trajectory results for the two different models were visually identical when plotted at the scale of a typical flight, apart from the existence of disc wobble at the very beginning of the trajectories for the exact case. Note that the mean value of the disc spin rate decreases in the exact model due to spin rate damping (C_{N_r}). However, based on a C_{N_r} value from Hubbard and Hummel, the spin rate is only reduced by approximately 3% during a typical 4-second flight. Since the present study is concerned with the overall trajectory behaviour, it was decided to use the constant spin rate model for all subsequent investigations.

The disc-wing mathematical model was implemented using Matlab 5.3 running on a 233 MHz Pentium PC. Equations of motion were solved numerically using the ODE23s solver in Matlab, with relative and absolute error tolerance set to default values of 1×10^{-3} and 1×10^{-6}, respectively. Typical simulation run times were of the order of 3 minutes for a 5 second flight for the constant spin rate model and 10 minutes for the exact model. Run time increased significantly with increasing advance ratio. The simulation was thoroughly debugged using a series of numerical experiments based on initial conditions for which the output trajectory could be easily predicted from simple physics. These experiments were designed to show that the implementation of the mathematical model was physically sound for all combinations of attitude and angle of attack. Example tests included horizontal release at zero forward speed, horizontal/vertical launch at zero angle of attack, launch at ±90° angle of attack, etc.

Results

Comparison with experimental data

A comparison between an experimental Frisbee trajectory from Hummel (2003) and a simulated trajectory from the same initial conditions is presented in Fig. 4. The results are qualitatively similar; however, the velocity magnitude for the simulated data shows a rapid decrease immediately following launch that is not present in the experimental data. This deceleration is

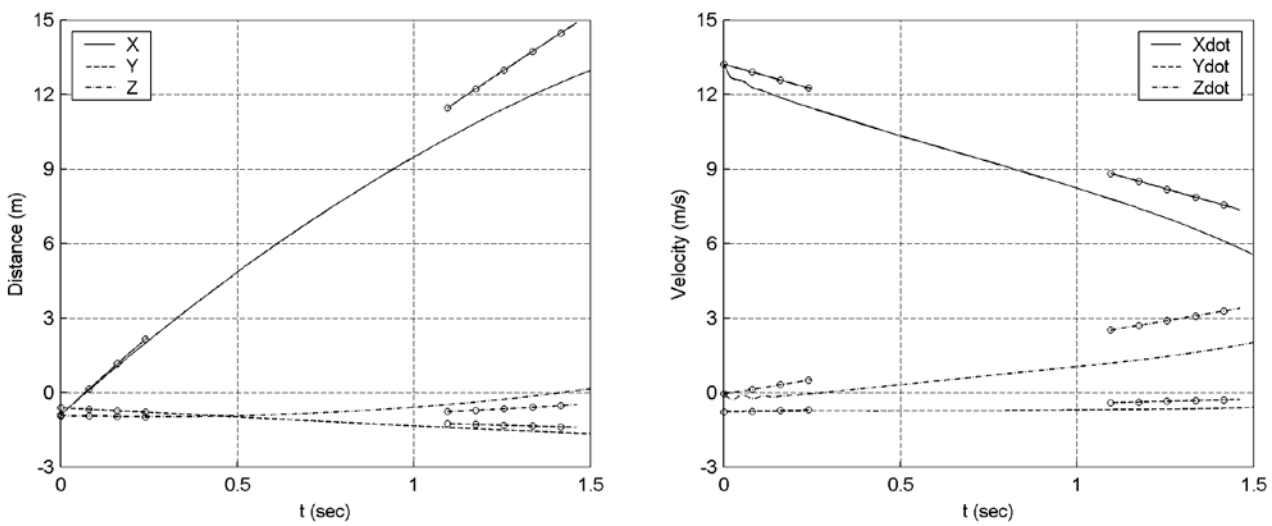

Figure 4 Comparison of simulated results (lines) with an experimental time history (lines + symbols) from a flight test (flight f2302; Hummel, 2003), for identical initial conditions given below.

X_L	Y_L	Z_L	u_L	v_L	w_L	ϕ_L	θ_L	ψ_L	p_L	q_L	r_L
m	m	m	m s^{-1}	m s^{-1}	m s^{-1}	rad	rad	rad	rad s^{-1}	rad s^{-1}	rad s^{-1}
–0.90	–0.63	–0.91	4.48	12.52	1.84	–0.07	0.21	5.03	–26.25	–5.19	52.85

caused by significant wobble of the disc following launch, which causes an oscillation in angle of attack of amplitude 15° and hence increase in drag. These conditions are not representative of a well-coordinated Frisbee throw. There is currently a lack of detailed published data on Frisbee trajectories and hence a clear need for further experimental data to provide a fuller validation of the simulation.

Analysis of a typical Frisbee trajectory

Trajectory plots and flight parameter time histories for a typical Frisbee trajectory are shown in Fig. 5. The disc (m = 0.175 kg, c = 0.275 m, $I_z = 2.4 \times 10^{-3}$ kg m^2) is launched at a pitch angle of 15° in the XZ plane (ϕ_L = 0°, θ_L = 15°, ψ_L = 0°) with a velocity of magnitude 15 m s^{-1} aligned with the x_1 axis, such that u = 15, v = 0, w = 0 m s^{-1} and the angle of attack is zero. The disc is spinning at 5 rev s^{-1} in a clockwise direction when viewed from above. The total flight time is 4 seconds, with discs shown in the trajectory plots every 0.2 seconds. Discs are drawn eight times their actual size. Black lines represent results from using the full non-linear aerodynamic model for the steady derivatives, grey lines represent results from using linearised derivatives.

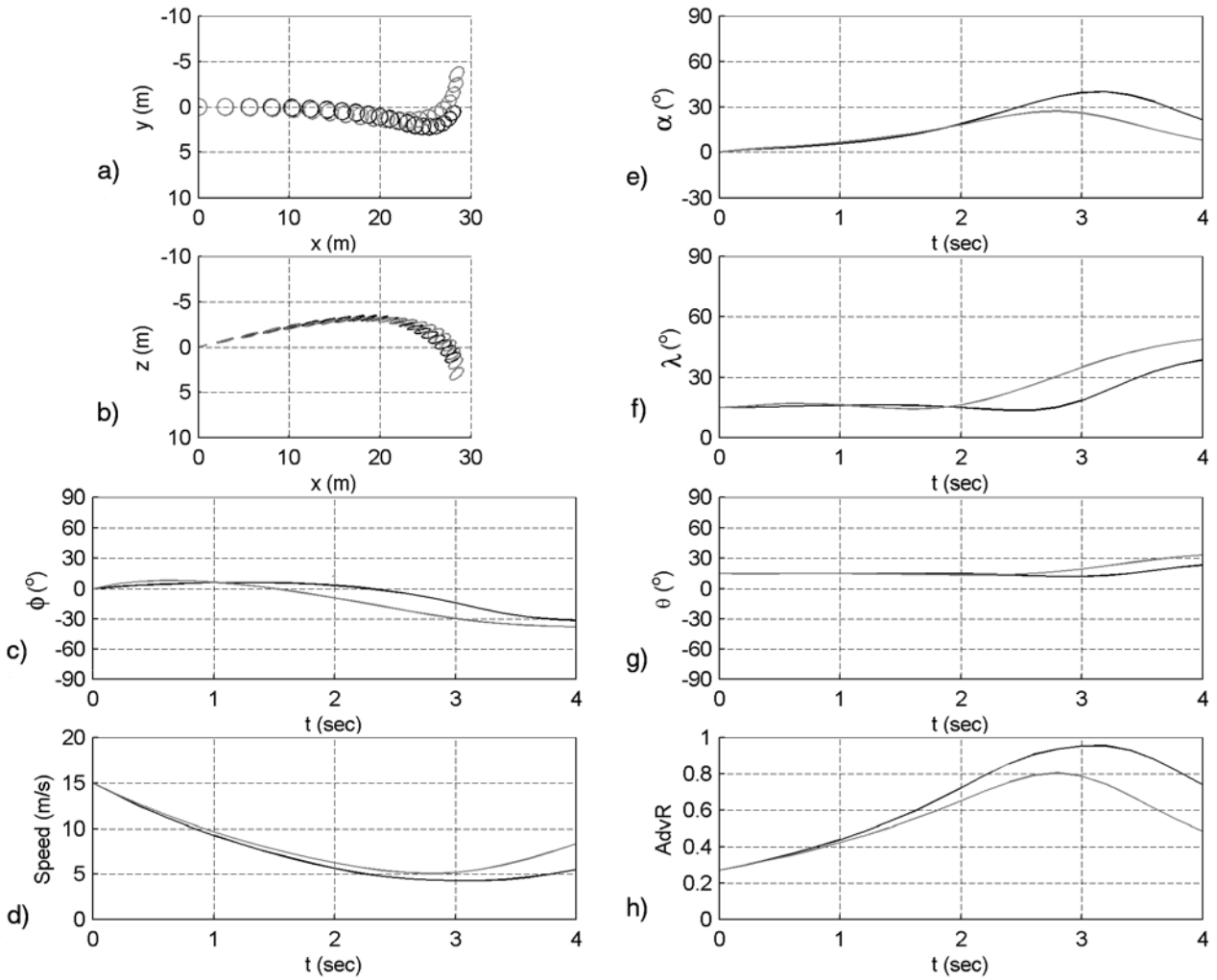

Figure 5 Trajectory plots and parameter time histories for a simulated Frisbee flight path. Solid lines correspond to results from using the full non-linear aerodynamic model. Grey lines correspond to results from using a linear approximation.
ϕ_L = 0°, θ_L = 15°, ψ_L = 0°, α_L = 0°, V_L = 15.0 m s^{-1}, $AdvR$ = 0.29

The full non-linear aerodynamic model case will be discussed first. The trajectory planform view in Fig. 5a shows the classic 'S' shaped flight profile associated with Frisbee flight in which the disc first turns one way, then turns the opposite way. This 'S' shaped profile arises from the relationship between pitching moment and angle of attack for the disc (Fig. 3c). At the start of the flight, with angle of attack close to zero, the pitching moment is negative. For a positive spin rate, this leads to a positive roll rate due to precessional effects (eqn. 54) and hence an increasingly positive roll attitude (Fig. 5c). As the flight progresses to around 2 seconds, the pitch attitude remains roughly constant (Fig. 5g), however the angle of attack is steadily increasing (Fig. 5e) due to the increased vertical velocity of the disc. When the angle of attack becomes greater than 9°, the pitching moment reverses sign and becomes positive, leading to a negative roll rate and hence an increasingly negative roll attitude. At around 3 seconds, the speed has reached a minimum point of around 4.5 m s^{-1}, the angle of attack has reached a maximum point of around 40°, and the disc is banked at an angle of around –15°. The disc then turns sharply to the left with the angle of attack decreasing and the absolute attitude increasing (Fig. 5f). Note that the advance ratio varies from 0.3 at the beginning of the flight to around 1 at 3 seconds due to changes in the disc flight speed over this period.

Focusing now on the linear aerodynamic case (grey lines and symbols), it can be seen that behaviour similar to the non-linear case is obtained initially, however, the rate of trajectory divergence increases appreciably after 2 seconds. This is due to larger differences in the aerodynamic models at increased angles of attack. The linear fit model diverges considerably from the wind tunnel pitching moment data (Fig. 3c) for angles of attack greater than 10°, as previously noted.

Effect of varying launch condition

Fig. 6 shows Frisbee trajectories in the XZ and XY planes for various launch initial conditions. The default initial condition is a launch attitude of ϕ_L, θ_L, ψ_L = [0 0 0]° and body axis velocity u, v, w = [19 0 0] m s^{-1}. Changes from these default conditions are indicated on each graph. The time interval between each data point is 0.2 seconds.

The effect of varying advance ratio at launch (obtained by varying spin rate, initial velocity held constant at 19.0 m s^{-1}) is shown in Fig. 6a and b. The non-dimensional analysis presented earlier predicts that the dimensionless roll rate of the disc increases with decreasing advance ratio, and the results in Fig. 6a qualitatively support this. At high advance ratios much greater than 1, the disc follows an almost straight path in the XY plane in line with the X axis. As the advance ratio decreases to around 0.4, the disc increasingly turns to the right, however the vertical motion is not much affected. At an advance ratio of 0.1, the increasingly positive roll attitude of the disc leads to an increasing rate of descent as the disc 'slips' out of the turn. Finally, at an advance ratio of 0, i.e. a non-spinning disc, the disc pitches leading edge down immediately after launch and descends with a tumbling motion in the vertical plane.

The next set of data (Fig. 6c and d) shows the effect of varying launch attitude. The XZ data (Fig. 6c) shows the classic 'boomerang' effect by which a disc can be made to return to the thrower if launched with sufficient pitch attitude. For the present case, a velocity reversal occurs for a launch pitch attitude of greater than 30°. Note that the data for this test were obtained at a high advance ratio of 1.1, so that the disc roll rate was minimised, and there is little lateral displacement in the XY plane (Fig. 6d). The relationships between launch pitch angle and maximum range is plotted in Fig. 7, and between launch pitch angle and maximum duration in Fig. 8. These results show that, based on the present simulation, the launch pitch angle for maximum range is approximately 10° and the launch pitch angle for maximum duration is approximately 20°. Note that range is much more sensitive to launch angle than is duration.

The effect of the launch angle of attack for a horizontally launched disc is shown in Figs. 6e and f. At zero angle of attack, the resulting trajectory is very similar to the zero launch attitude case in Fig. 6b, however, there is a slight difference due to the +3° offset of the aerodynamic angle of attack compared to the geometric angle of attack for the disc (see Fig. 3a). Note that the aerodynamic data for the full angle of attack range is present in the simulation (Potts, 2005), but is not included in Fig. 3. As the launch angle of attack is increased to 60°, the behaviour is qualitatively

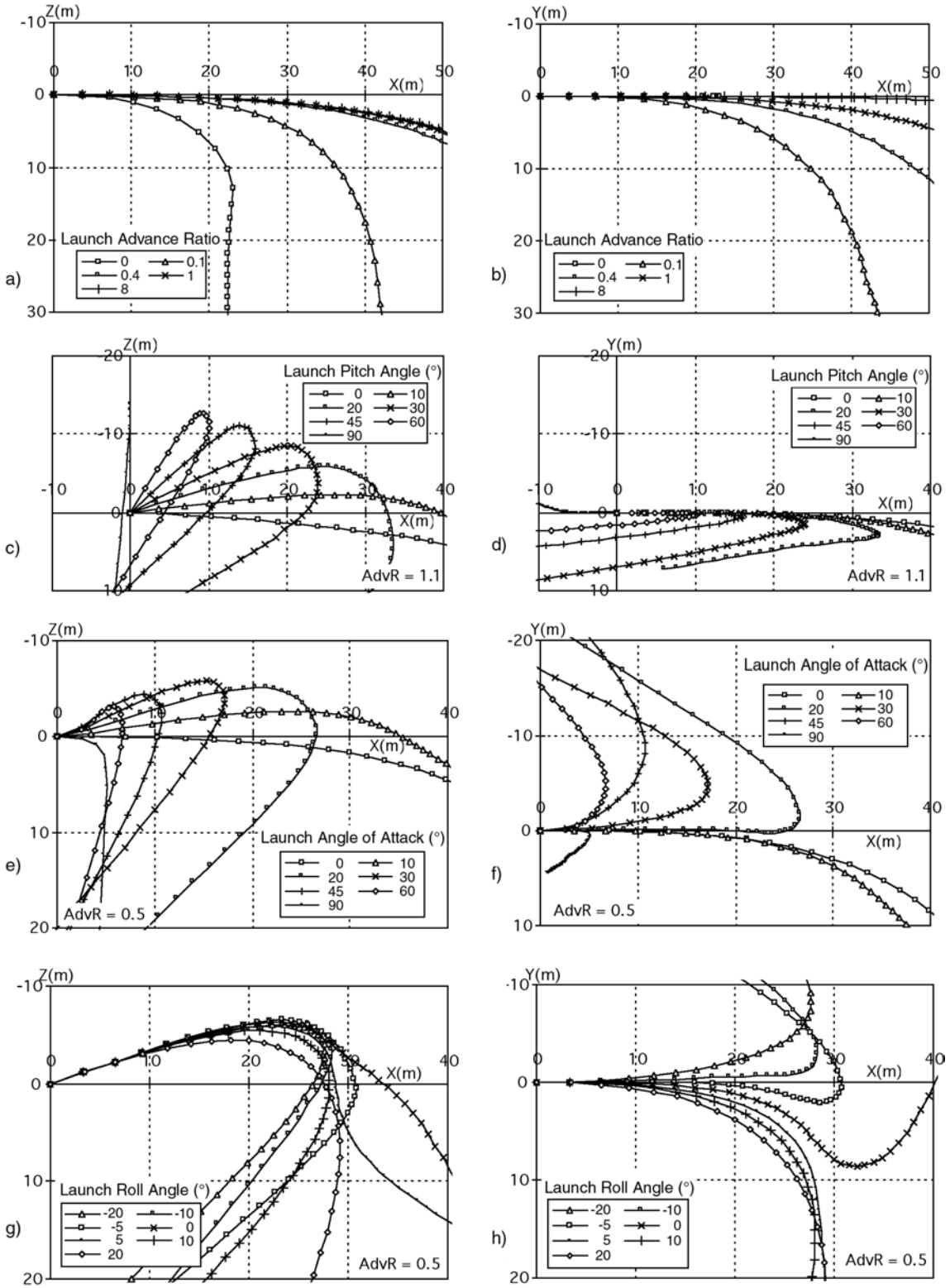

Figure 6 Effect of launch conditions (advance ratio, pitch angle, angle of attack and roll angle) on disc-wing XZ and XY trajectories. $V_L = 19.0$ m s^{-1}. Unless otherwise stated, $\phi_L = \theta_L = \psi_L = 0$.

similar to the effect of launch attitude, although both the range and duration are much reduced due to the effects of increased drag in the initial part of the flight. At a launch angle of attack of 90°, i.e. the disc is pitched to 90° and launched horizontally, the disc decelerates rapidly, immediately following a descending flight path, as would be expected. Note that the angle of attack tests were performed with an advance ratio of 0.5, and hence the lateral dispersion in the results is greater than in Fig. 6d.

The effect of launch roll attitude on the trajectory of a disc launched at zero angle of attack and a pitch attitude of 20° is shown in Figs. 6g and h. At zero roll attitude, the disc describes a classic 'S' shaped flight path. This is more pronounced than the 'S' profile shown in Fig. 5 since the advance ratio in the present case is reduced. By introducing a negative roll angle at launch, the initial curvature to the right is corrected, and an approximately straight initial flight path is achieved for a roll angle around –7°.

Of particular interest is the relationship between the landing spot of the disc, i.e. the XY location of the disc when $Z = 0$, and the launch roll angle, Fig. 9. Notice that the disc landing point follows an 'S' shaped locus starting on the left hand side of the X axis (from the point of view of a person standing at the launch point) and moving to the right hand side as the launch roll angle is changed from –30° to +30°. The locus is offset in that the landing point for zero roll angle is approximately 8 m to the right of the X axis. A landing closest to the X axis is achieved for an initial roll angle of approximately –6°.

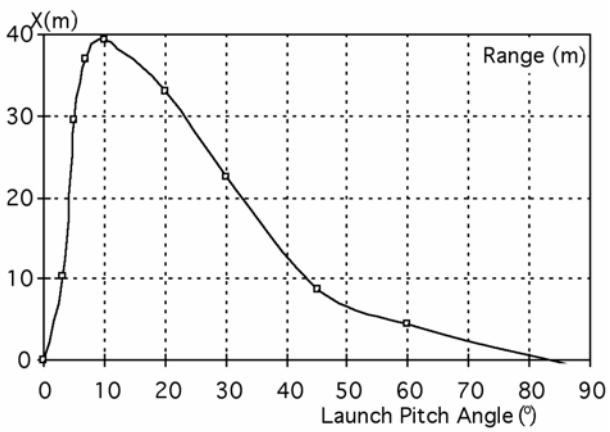

Figure 7 Range as a function of launch pitch angle. Maximum range occurs at around $\theta_L = 10°$.

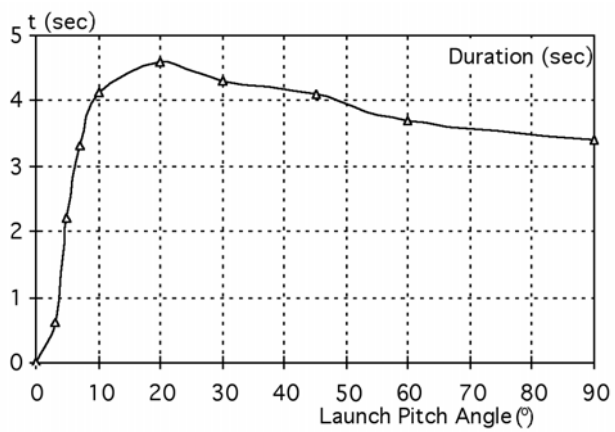

Figure 8 Flight duration as a function of launch pitch angle. Maximum duration occurs at around $\theta_L = 20°$.

Flight path similarity for similar dimensionless roll rates

It was proposed earlier (under 'Non-dimensional analysis') that dimensionless disc-wing flight trajectories are similar if the dimensionless roll rate is similar. In order to test this proposal, a number of numerical experiments were performed using a disc modelled as flat plate with the following parameters: $m = 0.015$ kg, $c = 0.06$ m, $I_z = 6.7 \times 10^{-6}$ kg m^2, $C_{Lift_a} = 2.46$,

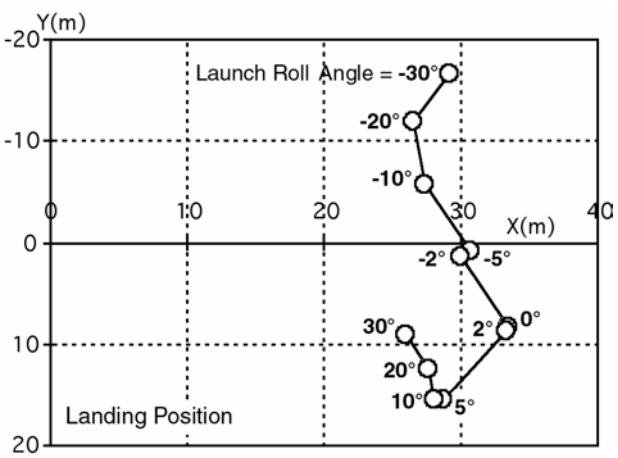

Figure 9 Disc landing position (XY location at which $Z = 0$) as a function of launch roll angle. Re-plotted from data in Fig. 6g, h.

C_{Drag_0} = 0.015, C_{Drag_a} = 2.80, C_{M_a} = 0.66 (Potts, 2005). The results of this investigation are shown in Fig. 10. The default initial condition is a launch attitude of ϕ_L, θ_L, ψ_L = [0 0 0]° and body axis velocity u, v, w = [15.7 0 0] m s^{-1}, with changes from these default conditions are indicated on each graph. Two cases are considered: the first (Fig. 10a) is used to simply demonstrate the validity of dimensionless length scales to collapse trajectories for geometrically and aerodynamically similar discs launched at different speeds. Note that in each case the speed and mass are varied such that at launch, lift = weight and that the static margin and advance ratio are constant, giving a dimensionless roll rate (eqn. 64) of –2.14. The second case (Fig. 10b) is used to demonstrate the validity of the dimensionless roll rate parameter. This is achieved by simulating trajectories for a number of discs with varying static margin and advance ratio with the constraint $k_n/AdvR$ = constant, such that $\hat{p}$ = constant. The high degree to which the dimensionless trajectories collapse in Fig. 10 suggests that the proposed dimensionless approach is sound and the proposed roll rate parameter is a potentially useful metric for comparing the flight characteristics of spin- stabilised disc wings.

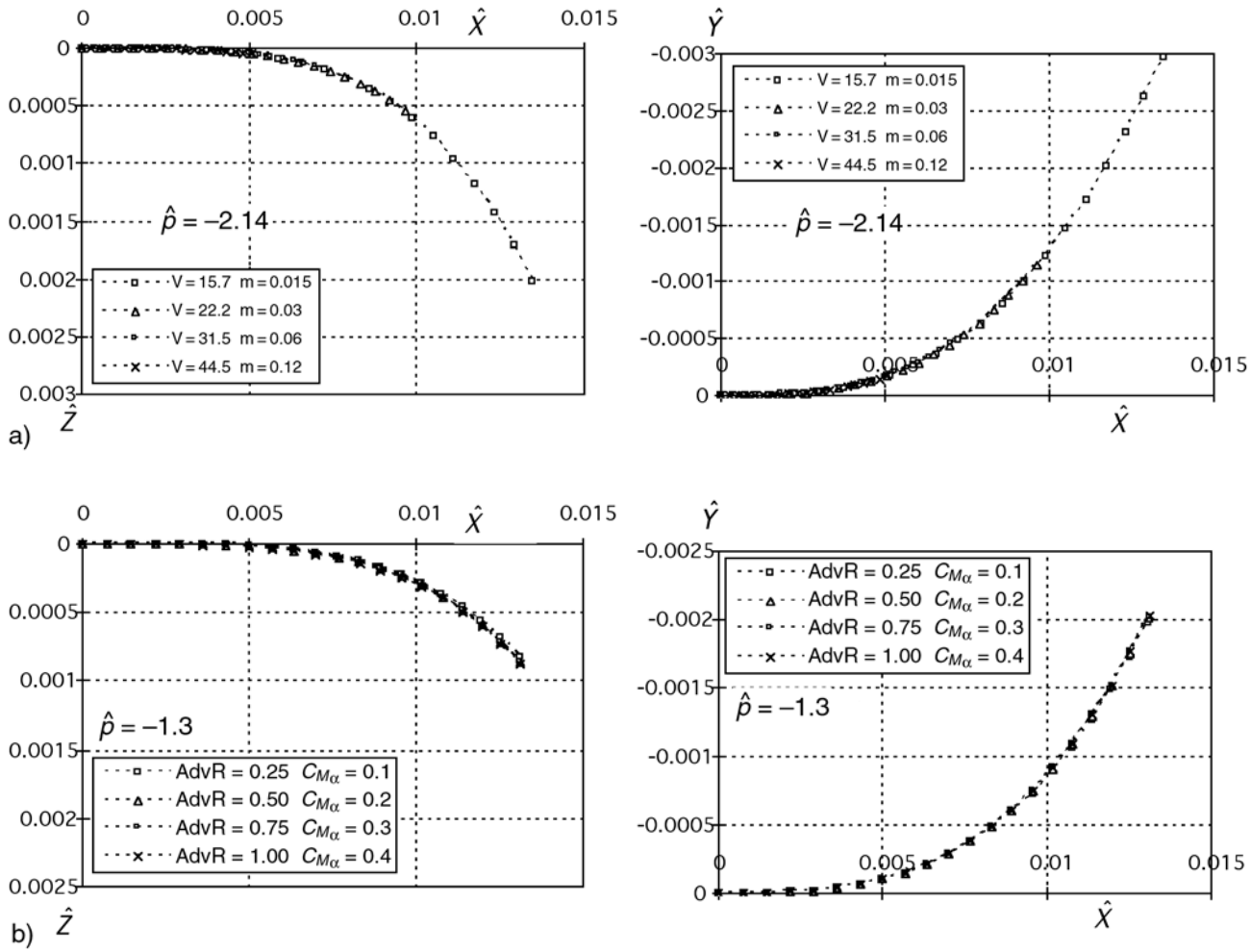

Figure 10 Validation of the use of the dimensionless roll rate as a trajectory similarity parameter. Dimensionless XZ and XY trajectory plots. First row, varying velocity and mass, $\hat{p}$ = constant = 1.3. Second row, varying advance ratio and C_{M_α}, $\hat{p}$ = constant = 0.47. Unless otherwise stated,

$\phi_L = \theta_L = \psi_L = 0°$, $\alpha_L = 2°$, $AdvR = 1$, $C_{Lift_\alpha} = 2.46$, $C_{M_\alpha} = 0.66$, $V_L = 15.7$ m s^{-1}, $m = 0.015$ kg.

Time interval between each data point is 0.1 seconds.

Disc-wing flight control

The original purpose of the work presented in this paper was to investigate the possibility of developing a steerable projectile based on a spin-stabilised disc-wing. For completeness, two examples of trajectories with fixed control inputs are discussed: firstly a downward spiral turn and secondly a spiral roll. It is envisaged that pitching moment inputs (and hence roll control) could be provided by cyclic variation of the centre line camber of the disc and hence varying C_{Mo}. Rolling moment inputs (and hence pitch control) could be provided by lateral variation of disc camber such that an asymmetric lateral load distribution is produced. As a less elegant alternative, small aerodynamic surfaces could be attached in a radial fashion to the edge of the disc and control moments produced via cyclic deflection of these, in a manner similar to the way in which control moments are produced by the main rotor on a helicopter.

Trajectory plots and parameter time histories for the spiral turn are shown in Fig. 11. The turn is set up by launching the disc at an initial bank angle of –45° and a pitch attitude of –30°, and by applying a constant control input rolling moment ($C_{Lcontrol}$ = 0.1)

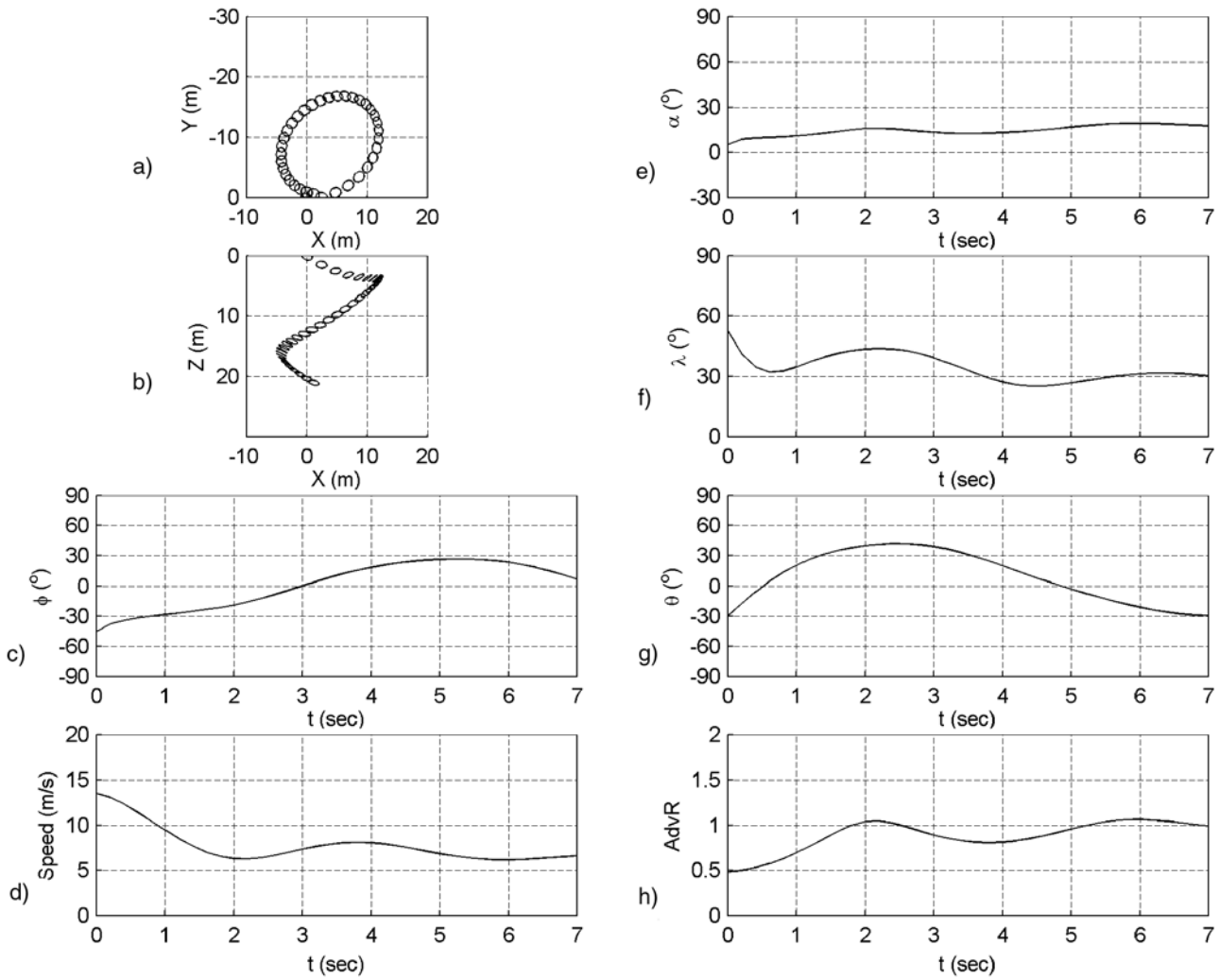

Figure 11 Trajectory plots and parameter time histories for a simulated spiral turn manoeuvre obtained using a constant rolling moment control input.

ϕ_L = –45°, θ_L = –30°, ψ_L = 0°, α_L = 5°, V_L = 13.5 m s^{-1}, $C_{Lcontrol}$ = 0.1, $AdvR$ = 0.5

introduced as an extra term in eqn. 22. From Fig. 11 it can be seen that after about 2 seconds the turn reaches approximately steady conditions, with an angle of attack of around 15°, an absolute attitude λ of around 30°, and a speed of around 7 m s^{-1}. Note that if the drag is set to zero, it is possible to launch the disc with a zero pitch attitude and a constant speed horizontal turn is achieved.

Trajectory plots and parameter time histories for the spiral roll are shown in Fig. 12. In this case, the manoeuvre is set up by launching the disc at a pitch attitude of –20° and an angle of attack of –3°, and by applying a constant pitching moment control input ($C_{Mcontrol}$ = 0.2) introduced as an extra term in eqn. 23. Note that the trajectory is such that the angle of attack remains constant at –3°, which is the angle of attack for zero lift. Since the angle of attack is constant, the lift to drag ratio of the disc is constant and hence the angle of the flight path in the XZ plane is constant, despite the velocity reducing.

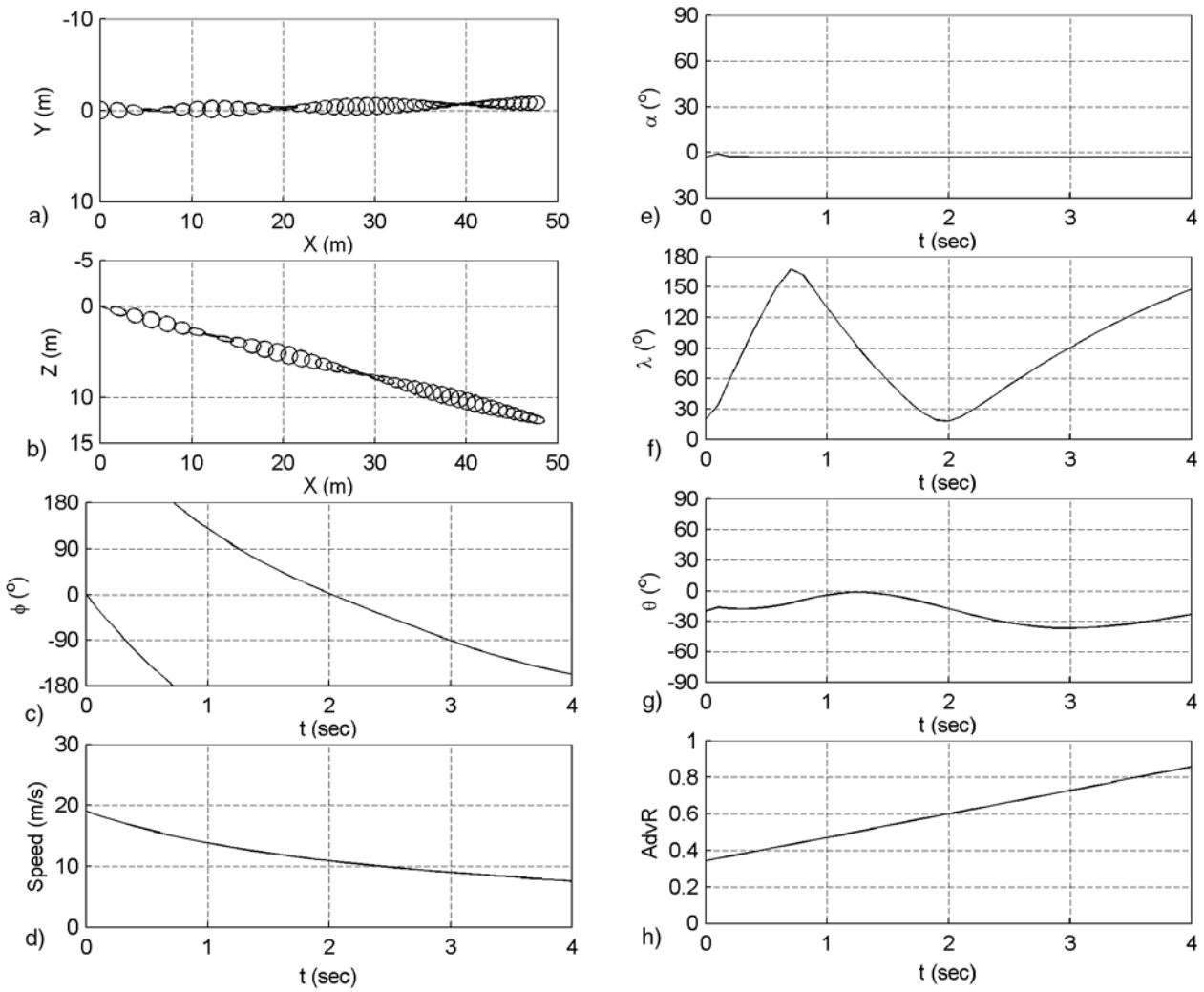

Figure 12 Trajectory plots and parameter time histories for a simulated spiral roll manoeuvre obtained using a constant pitching moment control input.

ϕ_L = 0°, θ_L = –20°, ψ_L = 0°, α_L = –3°, V_L = 19.0 m s^{-1}, $C_{Mcontrol}$ = 0.2, $AdvR$ = 0.34

Conclusions

A six degree of freedom mathematical model of a rotating disc-wing has been developed and a simplified analysis used to make predictions of the disc pitch and roll rate in response to aerodynamic moments. A dimensionless analysis of the roll rate equation has shown that dimensionless disc trajectories will be fundamentally similar if a parameter based on the ratio of the disc static margin to the disc advance ratio is similar.

The disc-wing mathematical model has been implemented successfully in Matlab, and it has been shown that the simulation can be simplified (and hence speeded up) without significant loss of accuracy by using a constant spin rate approximation. The simulation has been validated against a single experimental trajectory and reasonable agreement achieved. However, more flight test experimental data is needed to provide a more comprehensive validation database.

A comparison has been made between results for a typical throw trajectory based on using a non-linear aerodynamic model for steady terms and a model based on linear derivatives. The results are qualitatively similar, although differences increase for parts of the trajectory where the angle of attack is above around 10° due to inaccuracies in the linear pitching moment approximation.

The effect of a range of launch conditions has been investigated numerically. It is shown that:

- A high advance ratio (i.e. high disc spin rate) leads to straighter trajectories in the XY plane, as would be expected.
- The launch pitch angles for maximum range and maximum duration with ϕ_L = 0 are around 10° and 20° respectively.
- The effect of launch angle of attack is qualitatively similar to the effect of launch pitch attitude for angles of attack less than 60°. At higher angles of attack, increased drag at launch leads to greatly reduced range and duration.
- The locus of disc landing position as a function of launch roll angle for the typical launch pitch angle of 20° has been shown to be an 'S' shape curve, with the locus crossing the X axis for a roll angle of –6°.

The comparison of dimensionless flat-plate disc trajectories has provided evidence to support the proposed similarity relationship in that dimensionless disc-wing flight trajectories are similar if the dimensionless roll rate is similar. This suggests that the dimensionless roll rate is a fundamental parameter influencing the motion of a spin-stabilised free-flying disc.

Finally, it has been shown that with appropriate initial conditions and appropriate control moment input, it is feasible to explore hypothetical disc-wing manoeuvres such as a spiral turn and a spiral roll.

References

Bartlett, R.M. (1992) The Biomechanics of the Discus Throw: A Review, *J. Sports Sci.*, **10**, 467–510.

Etkin, B. & Reid, L.D. (1996) *Dynamics of Flight: Stability and Control*, John Wiley and Sons, 3rd Ed.

Frohlich, C. (1981) Aerodynamic Effects on Discus Flight, *Am. J. Physics*, **49**, 1125–32.

Hubbard, M. & Hummel, S. (2000) Simulation of Frisbee Flight, 5th Conference on Mathematics and Computers in Sport, G. Cohen (Ed.), University of Technology, Sydney, Australia, June 2000.

Hummel, S. & Hubbard, M. (2001) A Musculoskeletal Model for the Backhand Frisbee Throw, 8th International Symposium on Computer Simulation in Biomechanics, Politecnico di Milano, Milan, Italy, July 2001.

Hummel, S. & Hubbard, M. (2002) Identification of Frisbee Aerodynamic Coefficients using Flight Data, 4th International Conference on the Engineering of Sport, Kyoto, Japan, Sept. 2002.

Hummel, S.A. (2003) Frisbee Flight Simulation and Throw Biomechanics, PhD Thesis, Univ. California, Davis, USA.

Hummel, S. & Hubbard, M. (2004) Implications of Frisbee Flight Dynamics and Aerodynamics on Possible Flight Patterns, 5th International Conference on the Engineering of Sport, Davis, California, USA, Sept. 2004.

Katz, P. (1968) The Free Flight of a Rotating Disc. *Israel J. Tech.*, **6** (1–2), 150–155.

Lissaman, P.B.S. (1998) Disc Flight Dynamics, Unpublished Document, 29th Dec. 1998.

Lorenz, R.D. (2005) Flight and Attitude Dynamics Measurements of an Instrumented Frisbee, Measurement Science and Technology, Feb 2005.

Mitchell, T.L. (1999) The Aerodynamic Response of Airborne Discs, MS Thesis, University of Nevada, Las Vegas, NV, USA.

Nelson, R.C. (1982) *Flight Stability and Automatic Control*, McGraw-Hill, 2nd Ed.

Peterson, H. (1971) Calculation of Self-Suspended Flare Trajectories, Denver Research Institute, NAD/Crane RDTR No. 193, AD731866, 16 Sept. 1971.

Potts, J.R. & Crowther, W.J. (2002) Frisbee™ Aerodynamics, AIAA 2002–3150, 20th Applied Aero. Conf. & Exhibit, St. Louis, MI, USA, 24th–26th June 2002.

Potts, J.R. (2005) Disc-wing Aerodynamics, PhD Thesis, Univ. Manchester, UK.

Schuurmans, M. (1990) Flight of the Frisbee, *New Scientist*, 28th July, 37–40.

Soong, T.C. (1976) The Dynamics of the Discus Throw, *J. Appl. Mech.*, **98**, 531–6.

Stilley, G.D. & Carstens, D.L. (1972) Adaptation of Frisbee Flight Principle to Delivery of Special Ordnance, AIAA Paper No. 72–982.

Yasuda, K. (1999) Flight- and Aerodynamic Characteristics of a Flying Disk, *Japanese Soc. Aero. Space Sci.*, **47** (547), 16–22 (in Japanese).